THE JOURNAL OF BIOLOGICAL CHEMISTRY VOL. 288, NO. 17, pp. 12283–12294, April 26, 2013

Structural Analysis of the Regulation of the DYNLL/LC8 Binding to Nek9 by Phosphorylation*

Received for publication, February 5, 2013, and in revised form, March 8, 2013 Published, JBC Papers in Press, March 12, 2013, DOI 10.1074/jbc.M113.459149

Pablo Gallego[‡1], **Adrian Velazquez-Campoy**[§], **Laura Regué**[¶2], **Joan Roig**[¶3], **and David Reverter**[‡4]

From the [‡]*Structural Biology Unit, Institut de Biotecnologia i Biomedicina, Universitat Autònoma de Barcelona, 08193 Bellaterra, Spain, the* [§]*Department of Biochemistry and Molecular and Cell Biology and Institute of Biocomputation and Physics of Complex Systems (BIFI), Joint Unit IQFR, Consejo Superior de Investigaciones Científicas-BIFI, Universidad de Zaragoza, Spain, and Fundacion ARAID, 500018 Government of Aragon, Spain, and the* [¶]*Institute for Research in Biomedicine, 08028 Barcelona, Spain*

Background: Phosphorylation regulates binding of the mitotic kinase Nek9 to LC8, controlling signal transduction through the Nek9/Nek6/7 module.
Results: Crystal structures reveal the basis for the reduced interaction of LC8 for Nek9 upon phosphorylation on Nek9(Ser^{944}).
Conclusion: The reduced binding affinity of Nek9 for LC8 is due to diminished enthalpic interactions.
Significance: Disclosing phosphorylation as a novel mechanism that directly regulates LC8 protein-protein interactions.

The NIMA family protein kinases Nek9/Nercc1, Nek6, and Nek7 constitute a signaling module activated in early mitosis involved in the control of spindle organization. DYNLL/LC8 (dynein light chain 8) was originally described as a component of the dynein complex, but the recent discovery of multiple interaction partners for LC8 has suggested that it has a general role as a dimerization hub that organizes different protein partners. Recent experiments suggested that LC8 binding to Nek9 was regulated by Nek9 autophosphorylation on Ser^{944}, a residue immediately located N-terminal to the LC8 conserved (K/R)*x*-TQT binding motif, and that this was crucial for the control of signal transduction through the Nek/Nek6/7 module. In the present work, we present two crystal structures of LC8 with a peptide corresponding to the Nek9 binding region with and without a phosphorylation on Ser^{944}. Structural analysis of LC8 with both Nek9 peptides, together with different biophysical experiments, explains the observed diminished binding affinity of Nek9 to LC8 upon phosphorylation on Ser^{944} within the Nek9 sequence, thus shedding light into a novel phosphorylation regulatory mechanism that interferes with LC8 protein·protein complex formation.

Nek9 (also known as Nercc1) belongs to the mammalian NIMA family of protein kinases, named after the *Aspergillus nidulans* NIMA kinase (1). Mammals contain 11 members of the NIMA family or *Neks*, some of which are modular proteins with different protein domains, whereas some others only contain the kinase domain that has a sequence identity of ~40% for all members of the family (2). Mammalian *Nek* members seem to be specialized in functions related to the control of the microtubule and cilliary machineries (3). Nek6 and Nek7, together with Nek9, constitute a signaling module activated early in mitosis and involved in the regulation of the mitotic spindle (4). Nek9 (also called Nercc1) is a 120-kDa modular protein composed of an N-terminal kinase domain, with a strong sequence identity to the other members of the *Nek* family, followed by a domain homologous to RCC1 (the exchange factor for the small G protein Ran) and a C-terminal domain that contains a coiled-coil motif involved in dimerization (1). Nek9 is inactive during interphase and is activated at centrosomes and spindle poles during mitosis through a two-step mechanism involving CDK1 and Plk1 (1, 5, 6). In mitosis, Nek9 specifically interacts with the highly similar Nek6/7 (2, 7) and is able to directly phosphorylate and activate these two kinases (8). Thus, Nek9, together with Nek6 and Nek7, form a phosphorylation signaling module that is activated in mitosis and has been shown to be essential for correct mitotic progression, controlling spindle formation and different aspects of the centrosomal cycle during early mitosis (1, 4, 7, 9–11).

A recent report using two-hybrid experiments uncovered DYNLL/LC8 as a protein partner of Nek9 (12). LC8 was shown to interact with the C-terminal tail of Nek9, immediately after the coiled-coil region, in a conserved consensus motif (12). DYNLL/LC8 is a highly conserved ubiquitous eukaryotic protein with many protein partners involved in a great variety of cellular functions (13). Partners of LC8 include, among other proteins, dynein, myosin V, neuronal nitric oxide synthase, the proapoptotic protein BimL, and transcription factors Swallow and Trps1 (14–20). Although DYNLL/LC8 was initially proposed to be a cargo adapter for the molecular motor dynein and myosin V, the existence of multiple protein partners revealed LC8 as a regulatory hub protein that interacts with a linear consensus binding motif normally located in intrinsically disordered protein regions (21).

* This work was supported by "Ministerio de Ciencia e Innovacion" of Spain Grants BFU2012-37116 (to D. R.), BFU2010-19451 (to A. V. C.), and BFU2011-25855 (to J. R.) and European Community Grant MIRG-CT-2007-200346 (to D. R.).

The atomic coordinates and structure factors (codes 3ZKE and 3ZKF) have been deposited in the Protein Data Bank (http://wwpdb.org/).

[1] Supported by the Formación Personal Investigador fellowship from the "Ministerio de Ciencia e Innovacion" of Spain.

[2] Present address: Dept. of Molecular Biology and Medical Services, MA General Hospital and Dept. of Medicine, Harvard Medical School, Boston, MA 02115.

[3] Supported by the I3 program from the "Ministerio de Ciencia e Innovacion" of Spain.

[4] Supported by the Ramon y Cajal program from the "Ministerio de Ciencia e Innovacion" of Spain. To whom the correspondence should be addressed: Universitat Autonoma de Barcelona, 08193 Bellaterra, Barcelona, Spain. Tel.: 93-5868955; Fax: 93-5812011; E-mail: david.reverter@uab.cat.

Binding of LC8 normally promotes dimerization and a gain of structure of the protein partner, in some examples by facilitating the formation of coiled-coil structures immediately N-terminal to the LC8 binding region.

LC8 is a homodimeric structure that contains two hydrophobic binging grooves for linear peptides located in opposite sites of the central β-sheet interface (22). As shown by crystal structures of LC8 complexes, two peptides can interact simultaneously with the two hydrophobic grooves forming each one an extra β-strand to the central β-sheet of LC8 homodimer (23–25). Structural and functional data indicate that the homodimer structure of LC8 is essential for the interaction with protein partners, which are normally formed by dimeric structures (26, 27). Signaling inputs such as LC8 phosphorylation, pH variations, or the cellular redox state have been shown to regulate LC8 function by controlling its dimerization (28–30). Interestingly, it has been recently shown that phosphorylation of Ser^{88} in LC8, which promotes the disruption of the LC8 homodimer, can regulate the binding of protein partners such as dynein intermediate chain (27, 31).

Two different protein sequence motifs in target proteins can be recognized by LC8: (K/R)*X*TQT and G(I/V)QVD (where *X* is any amino acid) (32, 33). In addition to these short sequences, the binding region of the peptide can be extended at the N terminus, thus completing a total of nine residues forming the extra β-strand of the interface. Only a few LC8 partners contain non-canonical binding motifs lacking the most conserved Gln residue (25). The binding affinity of LC8 to monomeric peptides is moderately weak (K_d between 0.1 and 40 μM) (13); however, bivalent peptides linking two consensus motifs have been shown to increase significantly the binding affinity for LC8 (34), indicating the importance of the dimer-dimer interaction in the complex of LC8 with protein partners. Despite the strong conservation in the LC8 binding region, recent biophysical data indicates an inherent plasticity that allows the interaction with these different consensus motifs (24).

LC8 has been proposed to participate in the regulation of the Nek9/Nek6/Nek7 kinase signaling module as a negative regulator of Nek6/7 binding and activation (12). LC8 binding to the C-terminal region of Nek9 interferes with the interaction of Nek9 with Nek6 and Nek7, thus impeding Nek9 activation of Nek6/7. *In vivo* experiments suggest that autophosphorylation of Nek9 can regulate this process by regulating the binding of Nek9 to LC8. Ser^{944}, which is immediately located N-terminal to the LC8 consensus motif, has been proposed to be phosphorylated upon Nek9 activation and directly promote the LC8 dissociation from Nek9 *in vivo*, although such direct effect of Ser^{944} phosphorylation on LC8 binding has never been measured. The conservation in this position of a serine residue and the presence of other Ser/Thr residues in LC8 consensus motifs of many protein partners might indicate that phosphorylation could represent a general manner of regulation for the LC8 binding. To gain insights in this regulation, we have crystallized LC8 in complex with a Nek9 peptide corresponding to the LC8 binding region and with a similar phosphopeptide modified on the equivalent of Nek9(Ser^{944}). Comparison of both crystal structures sheds light into the diminished LC8 binding of Nek9 upon phosphorylation on Ser^{944}. Additionally, *in vitro* LC8 binding experiments using different biophysical methods demonstrate that phosphorylation on Ser^{944} reduces the affinity to form a complex with LC8, thus directly confirming that phosphorylation of the partner could be a general way to regulate interactions with LC8.

EXPERIMENTAL PROCEDURES

Protein Expression and Purification—The cDNAs encoding full-length LC8 and the Nek9-CC[5] constructs (Nek9, residues 893 to 974) were cloned into a pET28b vector with the fusion protein Smt3 tagged with six histidines at the N-terminal. Constructions were expressed in *Escherichia coli* BL21(DE3) for 4 h at 37 °C after induction with 1 mM isopropyl 1-thio-β-D-galactopyranoside, and recombinant proteins were purified by nickel-nitrilotriacetic acid agarose resin (Qiagen) and dialyzed against 20 mM Tris-HCl (pH 8.0), 250 mM NaCl, and 1 mM β-mercaptoethanol in the presence of SENP2 SUMO protease overnight at 4 °C. After protease cleavage, LC8 and Nek9-CC were purified by ion exchange chromatography using a Resource Q (GE Healthcare) column and by gel filtration using a Superdex75 column (GE Healthcare).

Single point mutants of NEK9-CC, including Q948A and S944E, were constructed using the QuikChange site-directed mutagenesis kit (Stratagene) according to the manufacturer's instructions. All sequences were sequenced after generation. Nek9-CC mutants were produced and purified as the wild-type form.

Peptide Design—The Nek9 peptide contains the amino acids between the Nek9 positions 940 to 950 resulting in the sequence VGMHSKGTQTA. In case of the Nek9 P-peptide, with a phosphate group on Ser^{944}, the resulting phosphopeptide contains the sequence VGMH(pS)KGTQTA. Both peptides were provided by the company Pepnome Limited.

Circular Dichroism—CD spectra were measured in a Jasco-715 spectropolarimeter thermostatted at 25 °C. Spectra were recorded from 260 to 200 nm at 0.5-nm intervals, 1-nm bandwidth, and scan speed of 10 nm/min. Ten accumulations were done for each spectrum. LC8 concentration for each scan is 11.2 μM buffered with 100 mM NaCl, 10 mM sodium phosphate, pH 7.5, and 1 mM β-mercaptoethanol. In each spectrum, we vary the Nek9 peptide or the Nek9 P-peptide concentration ranged between 0 and 26.6 μM.

In the case of LC8 binding to Nek9-CC (Nek9 residues from 893 to 974) wild-type and point mutants, LC8 and Nek9-CC concentrations were 10 μM and 6.66 μM, respectively, buffered as mentioned above. Same concentrations were used for the spectra of the LC8·Nek9-CC complexes. Data were normalized to [θ] (molar ellipticity) using the formula shown in Equation 1,

$$[\theta] = \theta \frac{1}{10 \cdot M \cdot N_e \cdot l} \qquad \text{(Eq. 1)}$$

where [θ] means molar ellipticity, θ indicates measured ellipticity, M represents molarity of the sample, N_e indicates the number of peptide bonds, and l indicates the cuvette path length in cm.

[5] The abbreviations used are: CC, coiled coil; SASA, solvent-accessible surface area.

Determination of the Interaction Constants (K_a) by Circular Dichroism—To determine the interaction constants between LC8 and the peptides, we measured the ellipticity at 220 nm in every spectrum. Because the interaction of LC8 with the peptides is characterized by moderate-to-high affinity and the concentrations are comparable with the expected dissociation constant, no approximation for the free ligand concentration can be made. The total concentration of ligand is expressed as follows:

$$[PL] = [P]_T \frac{K_A[L]}{1 + K_a[L]} \quad \text{(Eq. 2)}$$

where $[L]_T$ and $[P]_T$ are the total concentration of the peptide and LC8, respectively, K_a is the association constant, and $[L]$ is the concentration of the free ligand. Solving this equation for the unknown $[L]$ will allow calculating the concentration of the LC8·peptide complex, $[PL]$, for each experimental point,

$$[PL] = [P]_T \frac{K_a[L]}{1 + K_a[L]} \quad \text{(Eq. 3)}$$

from which the change in circular dichroism signal can be calculated in Equation 4,

$$Y = A_0 + A[PL] \quad \text{(Eq. 4)}$$

where A_0 is the circular dichroism signal at zero peptide concentration, and A accounts for the maximal change of the signal at high peptide concentration.

Thermal Denaturation of LC8 and LC8·Peptide Complexes—Thermal transition curves of LC8 and LC8·Nek9-peptide complexes were obtained in a spectrofluorometer (Cary Eclipse) at a heating rate of 0.2 °C/min following changes of intrinsic fluorescence at 338 nm while excited at 280 nm. The LC8 concentration was 11.2 μM in a buffer containing 100 mM NaCl, 10 mM sodium phosphate, pH 7.5, and 1 mM β-mercaptoethanol. To obtain the thermal denaturation curves for the LC8 in the presence of the two peptides, the experiments were performed in the presence of 11.2 μM concentration of the Nek9 peptide and P-peptide.

Thermodynamic Parameters from Thermal Unfolding—The thermal transition curves were fitted to obtain the unfolding thermodynamic parameters using Equation 5,

$$Y = (b_j + m_jT) + (b_u + m_uT)\frac{e^{((-\Delta H_m(1 - T/T_m))/RT)}}{1 + e^{((-\Delta H_m(1 - T/T_m))/RT)}} \quad \text{(Eq. 5)}$$

where m_j and b_j are the slope and the intercept with y axis in the pretransition region, m_u and b_u are the slope and the intercept with y axis in the post-transition region, ΔH_m is the unfolding enthalpy, T is the absolute temperature, T_m is the temperature at the melting point, and R is the universal gas constant.

Thermodynamic Binding Profile by Isothermal Titration Calorimetry—Binding interaction between LC8 and both peptides was assessed by high-sensitivity isothermal titration microcalorimeter AutoITC200 (MicroCal, GE Healthcare). Protein and peptide samples were properly degassed and carefully loaded into the cells to avoid bubble formation during stirring. Experiments were performed in 100 mM NaCl, 10 mM sodium phosphate, or Tris-HCl, pH 7.5, and 1 mM β-mercaptoethanol. Experiments were carried out titrating 20 μM LC8 in the calorimetric cell with 200–300 μM peptide in the injection syringe. The heat evolved after each ligand injection was obtained from the integral of the calorimetric signal. The heat due to the binding reaction was obtained as the difference between the reaction heat and the corresponding heat of dilution, and the latter was estimated as a constant heat throughout the experiment and included as an adjustable parameter in the analysis. The association constant (K_a) and the enthalpy change (ΔH) were obtained through non-linear regression of experimental data to a model for a protein with a single binding site. Data were analyzed using software developed in our laboratory implemented in Origin (version 7, OriginLab). The dissociation constant (K_d), the free energy change (ΔG), and the entropic change (ΔS) were obtained from basic thermodynamic relationships. Experiments performed in two buffers with different ionization enthalpies (0.86 kcal/mol phosphate, 11.4 kcal/mol Tris) allowed eliminating the contribution of proton exchange processes to the binding interaction and determining buffer-independent thermodynamic interaction parameters (enthalpy and entropy) (35, 36). Experiments performed at two temperatures, at 15 and 25 °C, allowed estimating the change in heat capacity upon binding, which is a binding parameter associated with changes in solvent accessible (polar and non-polar) surface area and, therefore, provides fundamental information on the binding interaction and possible conformational changes coupled to the complex formation.

Crystallization and Data Collection—Crystals of DYNLL/LC8 (dynein light chain 1) in complex with Nek9 peptide were obtained at 18 °C by sitting drop vapor diffusion methods. The reservoir solution contained 35% PEG 1500, 0.1 M MIB buffer (malonate, imidazole, and boric acid 2:3:3), pH 4. Crystals of LC8 in complex with Nek9 P-peptide were obtained at 18 °C by sitting drop vapor diffusion methods. The reservoir solution contained 30% PEG 1500, 0.1 M MIB buffer, pH 4.5. Single crystals appeared after 1 week from equal volumes of protein solution (12 mg/ml in 5 mM Tris, pH 8.0, 50 mM NaCl) and reservoir solution. All crystals were cryo-protected in reservoir buffer containing 15% glycerol and flash-frozen in liquid nitrogen prior to diffraction analysis. Diffraction data were recorded from cryo-cooled crystals (100 K) at the ALBA synchrotron in Barcelona (BL13-XALOC beamline). Data were integrated and merged using XDS (37) and scaled, reduced, and further analyzed using CCP4 (Table 1) (38).

Structure Determination and Refinement—The structure of LC8 in complex with Nek9 peptide and P-peptide were determined from the x-ray data by molecular replacement using a previous LC8 structure (Protein Data Bank code 2P1K) as a model. The initial electron density maps produced from molecular replacement programs were manually improved to build up complete models for LC8 and peptides using the program COOT (39). Model refinement was performed with Refmac (38) and Phenix (40). LC8 in complex with Nek9 P-peptide contained six LC8 molecules assembling three homodimers in the asymmetric unit, and the Ramachandran analysis shows 91.06%

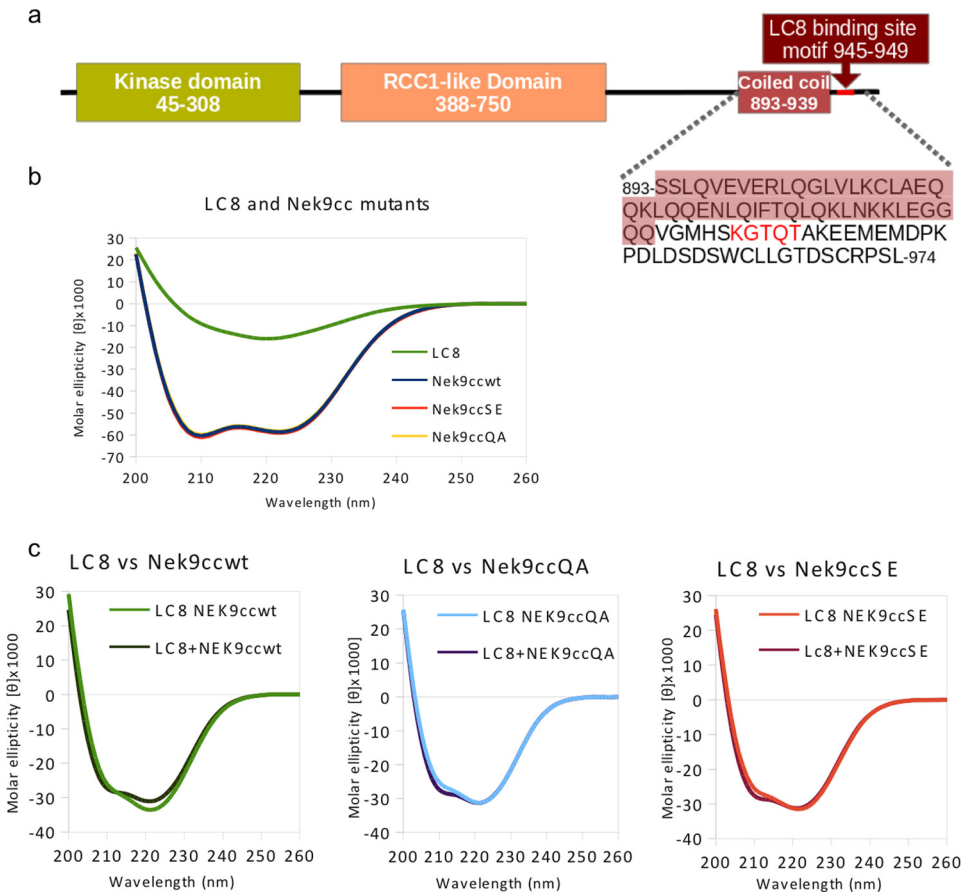

FIGURE 1. **Circular dichroism analysis of LC8 binding to the Nek9 C-terminal region.** *a*, schematic representation of the Nek9 protein. Amino acid sequence for the Nek9-CC construct is shown in one letter code. *b*, circular dichroism spectra of LC8 and Nek9-CC wild-type and single point mutants. *c*, circular dichroism spectra of the mixture of LC8 in complex with Nek9-CC and of the spectral sum of LC8 and Nek9-CC, for the Nek9-CC wild-type form and the Nek9-CC point mutants.

of residues (499 residues) are in preferred regions, 7.12% of residues (39) are in allowed regions, and 1.82% of residues (10) are in outlier regions. LC8 in complex with Nek9 peptide also contained six LC8 molecules assembled in three homodimers in the asymmetric unit, and the Ramachandran analysis shows 96.91% of residues (534 residues) are in preferred regions, 1.81% of residues (10) are in allowed regions, and 1.27% of residues (7) are in outlier regions. Refinement and data statistics are provided in Table 1. Structural representations were prepared with PyMOL (41).

Accession Codes—Coordinates and structure factors from the two structures were deposited in the Protein Data Bank with accession codes 3ZKE and 3ZKF.

RESULTS

Circular Dichroism Experiments on LC8 Binding to the Nek9 C-terminal Region—Dimerization of Nek9 has been proposed to occur by means of the predicted C-terminal coiled-coil region (residues 891–939), which is located immediately upstream of the LC8 consensus binding region (residues 940–950). In addition to Nek9 dimerization through its C-terminal coiled-coil region, LC8 has been suggested to contribute to Nek9 oligomerization as it does for other proteins (12). To analyze *in vitro* the interaction between LC8 and Nek9, CD experiments were carried out with LC8 and a fragment of the C-terminal region of Nek9, which includes the consensus LC8 binding region and the predicted coiled-coil region (Nek9-CC, residues 893–939) (Fig. 1). The concentrations of LC8 and Nek9-CC used in the CD experiments were 10 μM and 6.7 μM, respectively. CD spectra of the individual proteins show an expected α-β profile for LC8, and interestingly, a rich α-helix profile for the Nek9-CC fragment, which could be indicative of the presence of a coiled-coil structure. This is supported by the higher ordered multimeric structures that appear during the gel filtration purification of the recombinant Nek9-CC protein (12).

Remarkably, differences can be observed after comparison of the CD spectra of a mixture of the two proteins, LC8 and Nek9-CC, and the sum of their individual spectra (Fig. 1*C*). These changes in the ellipticity values between 200 and 240 nm suggest variations in the composition of secondary structure elements; in particular, the increase in ellipticity ~222 nm may indicate changes in the β/α structure. These results are in agreement with the previously reported binding between Nek9 and LC8 (12), and with crystal structures of LC8·peptide complexes, that indicated the formation of an extra β-strand (22).

To analyze the binding between LC8 and Nek9, we produced two Nek9-CC point mutant constructs. Nek9-CC Q948A can destabilize the binding by perturbing the highly conserved

Gln948 interaction with the LC8 dimer; and Nek9-CC S944E, a phosphomimetic that can destabilize the complex by mimicking phosphorylation on Ser^{944}, as it has been recently shown *in vivo* (12). Individual CD spectra of both Nek9-CC point mutants show similar profiles as the Nek9-CC wild-type form, probably indicating the formation of a coiled-coil structure (Fig. 1*B*). However, using the same protein concentrations as the wild-type form, the CD spectra of the mixture of LC8 with both Nek9-CC point mutants show differences in the CD profile compared with Nek9-CC wild-type, in particular in the region ~222 nm. This reduction in the ellipticity at 222 nm could indicate a decrease in the affinity of LC8 for both Nek9 mutant constructs under these experimental conditions. Thus, the destabilization of the binding with LC8 can occur either by the mutation on the conserved Gln^{947} residue, which has already been established to play an important role in LC8 binding, or by a mutation on Ser^{944}, a site proposed to regulate LC8 binding to Nek9 upon phosphorylation.

Crystal Structures of LC8 in Complex with Nek9 Peptide and Nek9 P-peptide—To gain insight at the atomic level into the Nek9 binding to LC8, we synthesized two different peptides corresponding to the Nek9 binding consensus region, with one of them carrying a phosphoserine modification at position 5 corresponding to position Ser^{944} in the Nek9 sequence, ^{940}VGMHSKGTQTA^{950}. Both peptides displayed good solubility properties and could be dissolved in aqueous buffers at relatively high concentrations. LC8 was also produced at milligrams level amounts, as reported previously (12). Purification of recombinant LC8 by gel filtration chromatography indicated unequivocally the presence of a homodimer organization in the quaternary structure of the protein.

Crystals of LC8 with both Nek9 peptides were produced in a similar reservoir condition but with different crystallographic space groups. Orthogonal protein crystals of LC8 with the unmodified Nek9 peptide diffracted beyond 2.2 Å resolution, whereas hexagonal protein crystals of LC8 with Nek9 P-peptide (phosphopeptide) diffracted at 2.6 Å resolution (see Table 1 for details). In both crystal forms, the asymmetric unit contained three homodimers, with each LC8 molecule bound to a Nek9 peptide (a total number of 12 distinct molecules form the asymmetric unit). Both Nek9 peptides could be completely traced in the electron density maps in the three homodimers and only in some cases lacked the flexible terminal residue.

Both crystal forms display a similar LC8 homodimeric structure, which constitutes the biological unit and has been well established in the recent years by different structures, either in the apo form or in complex with peptides (13, 22–25). Basically, the LC8 structure is composed by two monomers with a characteristic fold formed by five five-stranded antiparallel β-sheets at the center of the homodimer, swapping four strands from one monomer with a fifth strand from the other monomer (Fig. 2*A*). Additionally, each LC8 monomer contains a pair of α-helices flanking the central β-sheet region at opposite faces of the homodimer. The peptide-binding region is located in identical opposite grooves at the two edges of the dimerization interface. As observed in other LC8 complex structures, the bound peptide interacts in an extended orientation and forms an extra β-strand with LC8, increasing the total number of strands of the central β-sheet. The parallel orientation of the two Nek9 peptides in the LC8 homodimer would be compatible with the presence of the coiled-coil structure immediately before the LC8 binding region (Fig. 2*A*).

TABLE 1
Data collection and refinement statistics
Statistic for highest resolution shell is shown in parentheses.

	LC8·Nek9 peptide	LC8·Nek9 P-peptide
Data collection		
Space group	$P2_12_12_1$	$P6_3$
a, *b*, *c* (Å)	39.98, 105.12, 133.89	154.86, 154.86, 47.72
α, β, γ	90.00°, 90.00°, 90.00°	90.00°, 90.00°, 120.00°
Resolution (Å)	44.63–2.20 (2.32–2.20)	47.73–2.50 (2.63–2.50)
Rmerge[a]	0.080 (0.53)	0.100 (0.95)
$I/\sigma I$	8.0 (2.7)	7.6 (1.5)
Completeness (%)	97.6 (95.4)	99.2 (95.6)
Redundancy	3.2 (3.1)	3.4 (3.3)
Refinement		
Resolution (Å)	82–2.2	45–2.6
No. of reflections	27,276	19,327
R_{work}/R_{free}[b]	19.73/22.76	21.96/26.86
No. of atoms	4726	4671
Protein	4619	4650
Water	107	19
r.m.s. bond lengths (Å)[c]	0.02	0.01
r.m.s. bond angles	1.92°	1.19°

[a] $R_{merge} = \Sigma|I_i - \langle I\rangle|/\Sigma I_i$, where I_i is the *i*th measurement of the intensity of an individual reflection or its symmetry-equivalent reflections and $\langle I\rangle$ is the average intensity of that reflection and its symmetry-equivalent reflections.
[b] $R_{work} = \Sigma||F_o| - |F_c||/\Sigma|F_o|$ for all reflections and $R_{free} = \Sigma||F_o| - |F_c||/\Sigma|F_o|$, calculated based on the 5% of data excluded from refinement.
[c] r.m.s., root mean square deviation.

As observed in previous LC8·peptide complexes, the Nek9 peptide and Nek9 P-peptide interact extensively with the central β-sheet of the LC8 homodimer (Figs. 2 and 3), establishing several backbone hydrogen bonds and side chain interactions with the β3 strand of one of the LC8 subunit. The only interaction of the peptide with the opposite subunit of the LC8 homodimer is mainly established by Gln^{947} from the highly conserved K*X*TQT*X* motif, with its side chain buried in a hydrophobic pocket formed by Ile^{34}, Glu^{35}, and Lys^{36} from the α2 helix.

Most of the interactions are basically conserved between in both complex structures, although two hydrogen bonds are disrupted in the Nek9 P-peptide structure. In particular, the backbone hydrogen bond of the carbonyl group of Gly^{941} is not formed in some of P-peptide molecules found in the asymmetric unit. A second disrupted interaction is the hydrogen bond between Ser^{944} and Thr^{67} (at 2.69 Å in the case of the Nek9 peptide structure), which is in all cases disrupted by the presence of the phosphate group at Ser^{944}. The phosphate group of Ser^{944} is located at the homodimer interface, in contact with the side chain of Tyr^{65}, from the β3 strand, and next to the side chains of Lys^{43} and Lys^{44} from the opposite LC8 subunit (Fig. 2).

Interestingly, structural superposition of the six different peptides found in the asymmetric unit show that the Nek9 P-peptides display a high degree of flexibility when compared with the unmodified Nek9 peptides, which displays an almost identical superposition of peptides (Fig. 3). This increase of flexibility displayed by the Nek9 P-peptide is more prominent at the N-terminal part of the P-peptide (from Val^{940} to His^{943}), compared with the K*X*TQT*X* C-terminal part (from Lys^{945} to Thr^{949}). These results suggest that phosphorylation on Ser^{944},

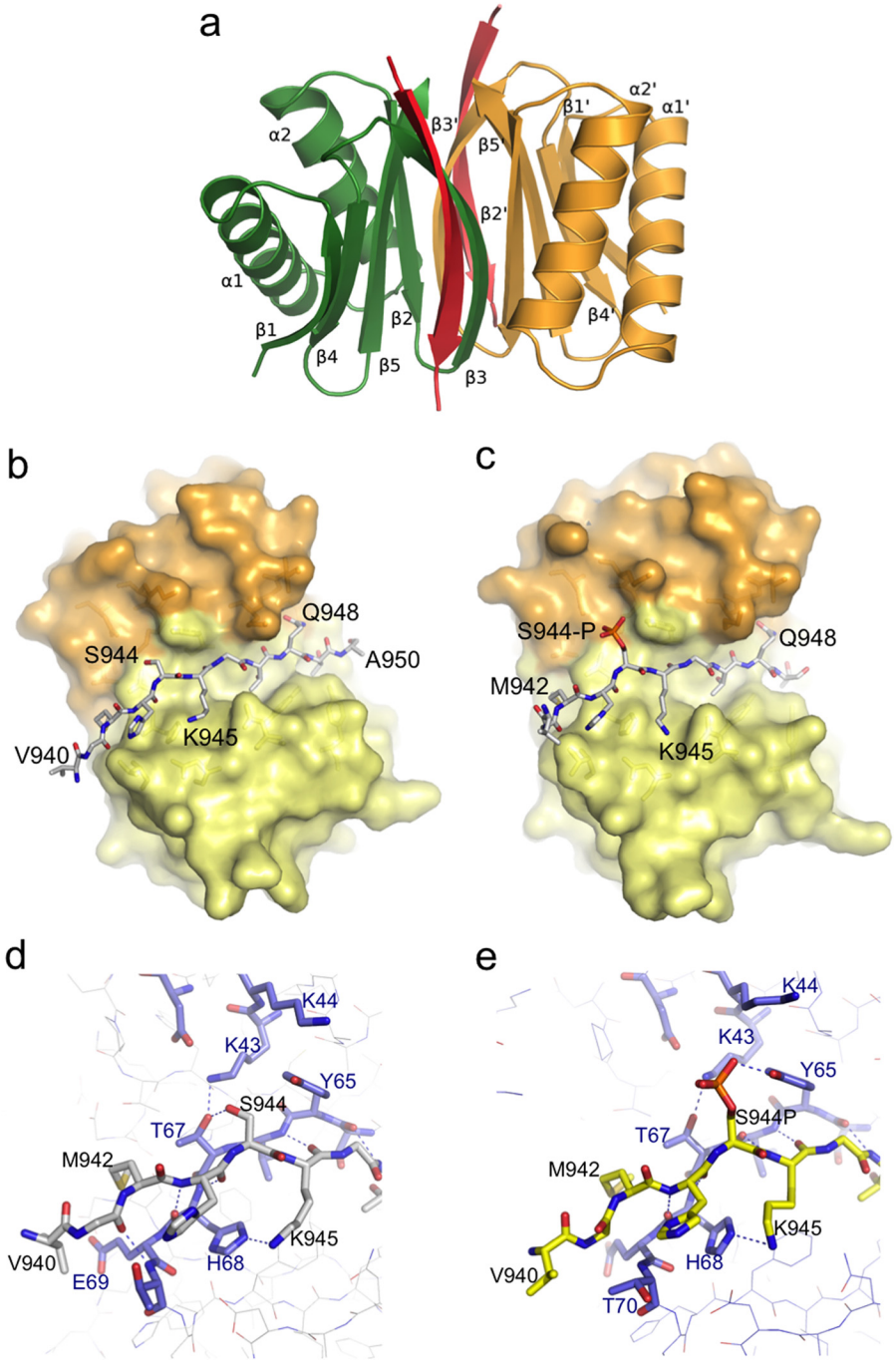

FIGURE 2. **Crystal structures of LC8 with Nek9 peptide and Nek9 P-peptide.** *a*, schematic representation of the LC8·Nek9 peptide structure. α-Helices and β-strands of each LC8 subunit are labeled. The two Nek9 peptides binding the homodimer are depicted in *red*. *b*, surface representation of the LC8 homodimer (*yellow* and *orange*) in complex with the Nek9 peptide, which is labeled and shown in stick representation. *c*, surface representation of the LC8 homodimer (*yellow* and *orange*) in complex with the Nek9 P-peptide, which is labeled and shown in stick representation. *d*, detailed stick representation of the interaction between the N-terminal regions of the Nek9 peptide (*gray*) with LC8 (*blue*). *e*, detailed stick representation of the interaction between the N-terminal region of the Nek9 P-peptide (*yellow*) with LC8 (*blue*). The figure was prepared with PyMOL (43).

which is located four positions N-terminal to the central Gln^{948}, affects the interaction of the Nek9 peptide to LC8 by producing a destabilization of the complex. Our detailed structural analysis supports the hypothesis that phosphorylation on Ser^{944} can modulate and weaken the binding of LC8 to Nek9 in the cellular context, in which protein concentrations are much lower than in crystal structures and the phosphorylation outcome may be more evident.

Another remarkable difference found after comparison of both crystal structures is a shift produced in the LC8 homodimer structure upon binding to the Nek9 P-peptide, in particular in one of the LC8 monomers with respect to the other monomer (Fig. 3*C*). This shift might be attributed to the presence of a phosphate group at Ser^{944}, in which its negative charge might somehow interfere in the dimer interface. It is possible that the lysine residues from the opposite subunit next to the phosphate group are affected by the

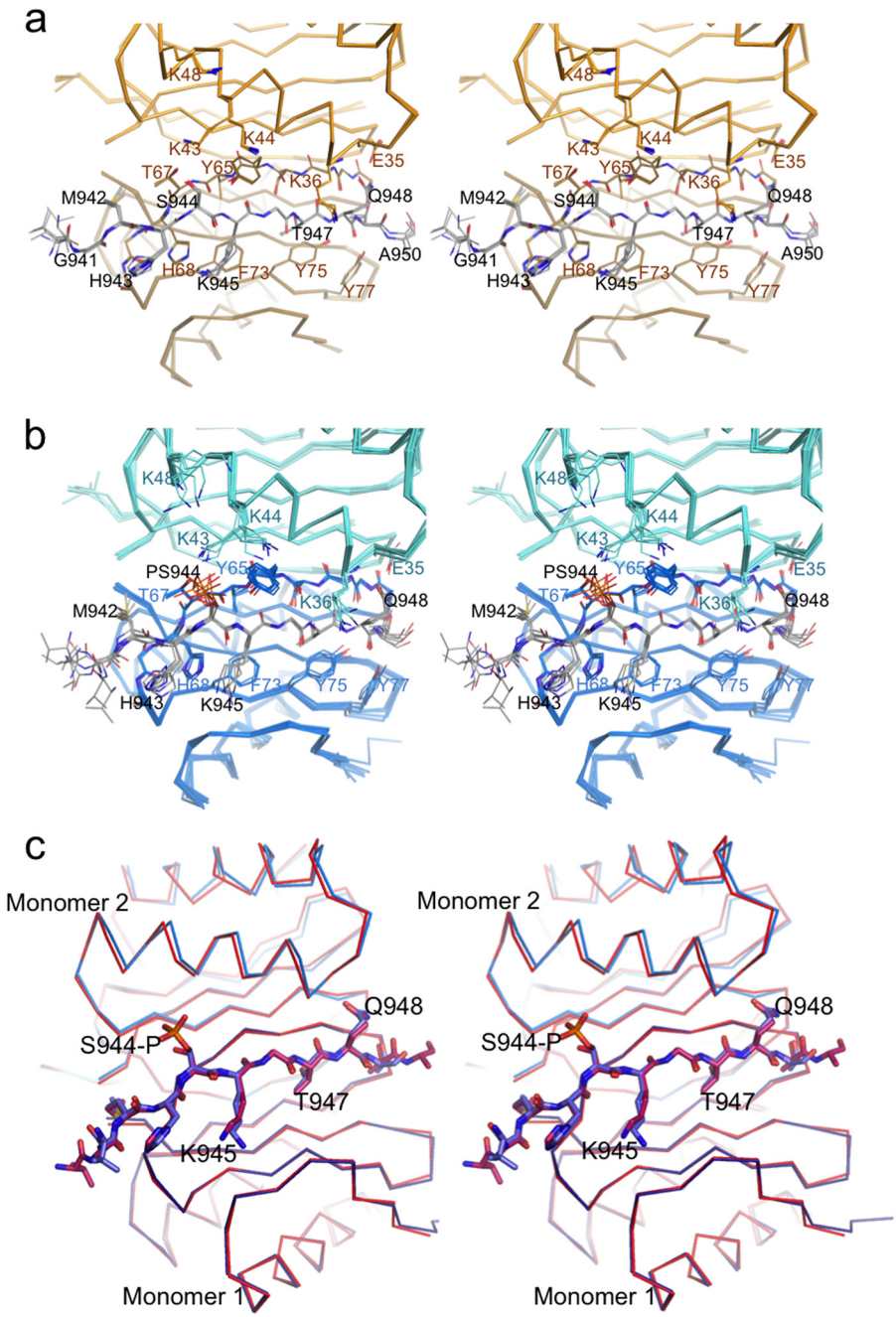

FIGURE 3. **Comparison of the interaction of LC8 with Nek9 peptide and Nek9 P-peptide.** *a*, stereo representation of the superposition of the six Nek9 peptides from the asymmetric unit. Nek9 peptide and interacting LC8 residues are labeled and shown in stick representation. *b*, stereo representation of the superposition of the six Nek9 P-peptides from the asymmetric unit. Nek9 P-peptide and interacting LC8 residues are labeled and shown in stick representation. *c*, stereo representation of the ribbon superposition of the LC8·Nek9 peptide and LC8·Nek9 P-peptide structures. Both Nek9 peptides are labeled and shown in stick representation. The two LC8 subunits of the homodimer are labeled monomers 1 and 2.

negative charge of the phosphate group. In contrast to the structural comparison between LC8· neuronal nitric oxid synthase and LC8·Swa complexes (42) and despite the aforementioned LC8 subunit shift, we have not observed an enlargement of the peptide-binding cleft in the Nek9 P-peptide complex. This movement in the homodimer quaternary structure upon Ser^{944} phosphorylation could be significant to perturb the binding and stability of the Nek9 peptide to LC8.

Circular Dichroism Experiments of the Binding of LC8 to Nek9 Peptides—Because the binding partners increase the β-sheet signal by adding an extra strand to the central five-stranded β-sheet of LC8, CD represents an appropriate method to calculate the binding affinity in titration experiments. The CD spectrum of LC8 shows a characteristic curve for a α/β-rich protein, displaying a maximal negative ellipticity value ~220 nm (Figs. 1*B* and 4). Using fixed LC8 concentrations, titration experiments were conducted by measuring the CD spectra of increasing concentrations of the unmodified Nek9 peptide (Fig. 4*A*). The observed augment of the ellipticity ~220 nm, which signals changes in the α/β-secondary structure, might indicate an increase of β-structure produced by the binding of the Nek9 peptide. CD spectra comparisons indicate a major increase of

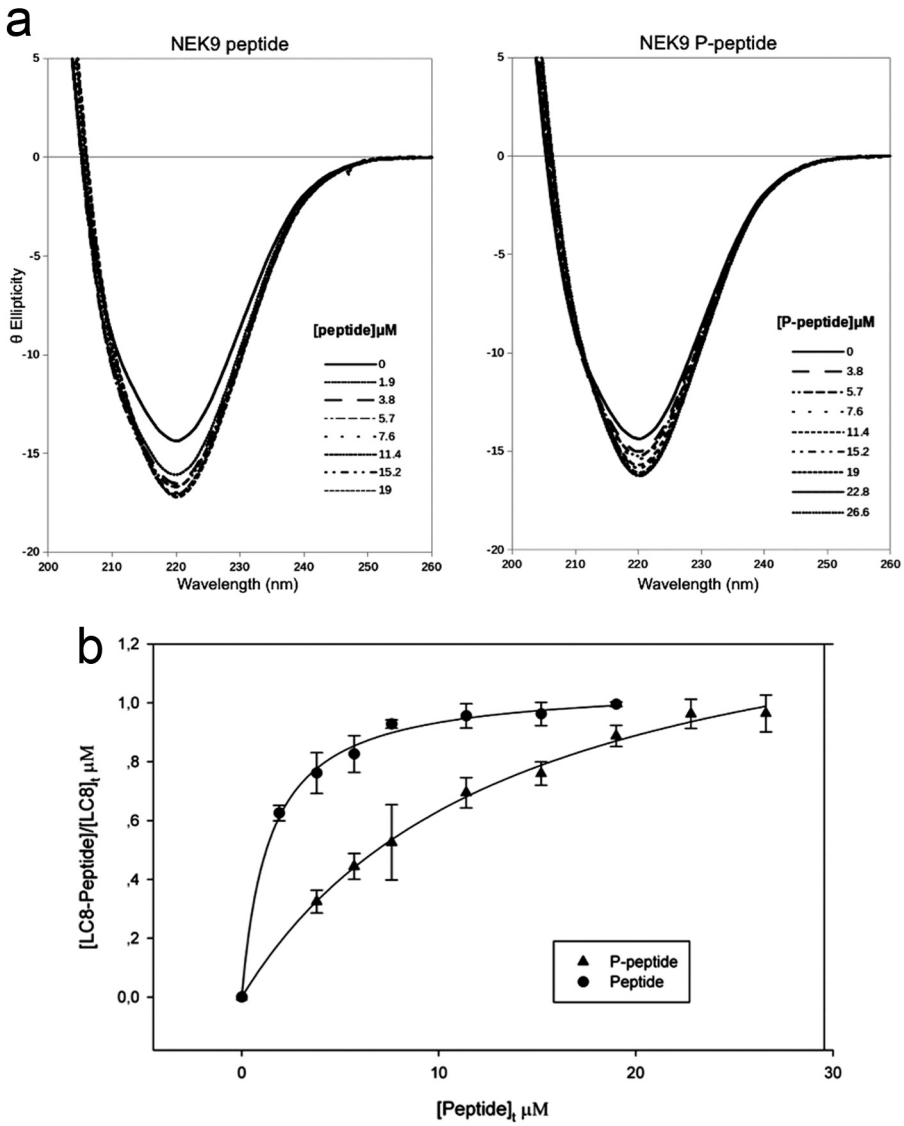

FIGURE 4. **Circular dichroism analysis of LC8 binding to Nek9 peptide and Nek9 P-peptide.** *a*, *right*: circular dichroism spectra of the titration of LC8 with an increasing concentration of the Nek9 peptide. *Left*: circular dichroism spectra of the titration of LC8 with an increasing concentration of the Nek9 P-peptide. *b*, plot of the variation of the ellipticity values from the CD spectra of *a* and *b* at 220 nm, which follows the change of β-secondary structure. *Circles*, Nek9 peptide; *squares*, Nek9 P-peptide.

the β-signal between 0 and 1.9 μM peptide concentration (Fig. 4*A*).

When identical CD titration experiments were carried out with the Nek9 P-peptide, a smaller increase in β-signal was observed, in contrast to the unmodified Nek9 peptide (Fig. 4*A*). The LC8 titration with the Nek9 P-peptide shows a smoother increase at 220 nm and, unlike the unmodified Nek9 peptide, the signal is not saturated ~1.9 μM. The β-signal of the Nek9 P-peptide spectra seems to increase more gradually, probably indicating a reduced binding affinity of the Nek9 peptide upon phosphorylation.

To calculate the different binding capabilities between the two peptides, the change in ellipticity at 220 nm has been represented as a function of the increase of peptide concentration (phospho- and unmodified Nek9 peptide) (Fig. 4*B*). The two curves were analyzed considering that the concentrations of protein and peptide are comparable (see "Experimental Procedures"), and the dissociation constant (K_d) for each peptide was determined. Using this approach, we have estimated K_d values ~ 0.2 and 3.7 μM for the unmodified and the Nek9 P-peptide, respectively, thus confirming our hypothesis that the unmodified peptide binds tightly to LC8. These K_d values are in the range of reported LC8-peptide interactions (13) and suggest that phosphorylation of the Nek9 peptide results in a 18-fold reduction of binding to LC8, thus supporting conclusions drawn from crystal structures.

Thermal Denaturation of the LC8·peptide Complex—Protein stability of the LC8·peptide and LC8·P-peptide complexes was analyzed by changes of the intrinsic fluorescence during thermal denaturation. Based on our CD experiments, fixed concentrations of Nek9 peptides (11 μM) were chosen to form a complex with LC8. At this concentration, CD analysis showed a partial binding of the Nek9 P-peptide to LC8 in comparison with the Nek9 peptide at 20 °C. The transition curves of the heat-induced fluorescence emission changes of LC8 complexes are shown in Fig. 5. These curves include LC8 alone,

and LC8·peptide and LC8·P-peptide complexes. Single cooperative transition curves were observed, and the data were fitted to a two-state temperature-induced protein-unfolding model (all curves with $R > 0.999$). As shown in Table 2, the transition temperatures of unfolding obtained for the three curves are quite similar (T_m ~333 K), indicating minor changes produced in the context of a global denaturation. However, the different extracted thermodynamic enthalpies support the existence of significant differences for both Nek9 peptides (Table 2).

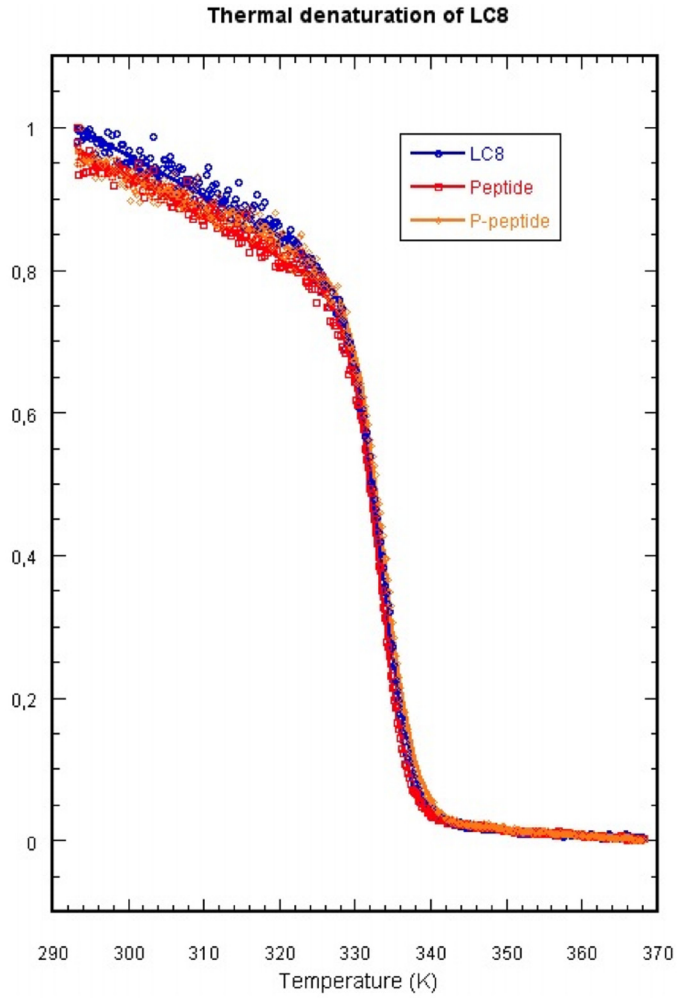

FIGURE 5. **Thermal unfolding of LC8 followed by intrinsic fluorescence.** *Blue circles* indicate the thermal unfolding kinetic of LC8 *Red squares* indicate the thermal unfolding kinetic of LC8 in the presence of 11 μM Nek9 peptide. *Orange diamonds* indicate the thermal unfolding kinetic of LC8 in the presence of 11 μM Nek9 P-peptide.

TABLE 2

Parameters from the thermal unfolding of the LC8·Nek9 peptide complexes

	LC8	LC8·Nek9 peptide	LC8·Nek9 P-peptide
T_m (K)	333.4 ± 0.1	333.1 ± 0.1	333.8 ± 0.1
ΔH_m (kcal/mol)	158 ± 2	174 ± 2	156 ± 2

In the case of LC8 alone and LC8·Nek9 P-peptide complex, the enthalpies for the thermal denaturation unfolding experiments are comparable, ~156.8 and 155.8 kcal/mol for each, respectively. However, these similar values are in contrast with the higher enthalpy value (~174.2 kcal/mol) shown for the LC8·Nek9 peptide complex. This higher enthalpy value could be an indication of a large number of disrupted bonds during the denaturation experiment, thus suggesting the formation of a tighter complex between LC8 and Nek9 peptide that would support our previous observations.

Thermodynamic Profile of the LC8 Complex Formation—Thermodynamic binding parameters for LC8 in complex with the two Nek9 peptides were determined by isothermal titration calorimetry. Experiments performed in two buffers with different ionization enthalpies indicated that the binding of the peptides is coupled to a minor proton uptake process. (The number of exchanged protons, n_H, is small and positive (Table 3).). Titration experiments of both Nek9 peptides on LC8 showed that the affinity of the Nek9 P-peptide for LC8 is reduced by ~6-fold in the dissociation constant (K_d is 0.16 and 0.96 μM, for both Nek9 peptide and P-peptide, respectively) (Fig. 6). This decrease of the K_d in the Nek9 P-peptide is due to a reduction of the enthalpy in the complex with LC8 (Table 3), probably by a reduced number of bonds formed between LC8 and Nek9 peptide.

Thus, the decrease of the affinity for LC8 for the Nek9 P-peptide is basically caused by less favorable enthalpic interactions ($\Delta\Delta H$ = 1.7 kcal/mol) combined by a partial compensation from more favorable entropic interactions ($-T\Delta\Delta S$ = −0.6 kcal/mol) (Table 3). These two factors produce a global reduction of the affinity, as observed in the difference of the binding Gibbs energy value ($\Delta\Delta G$ = 1.1 kcal/mol), producing the aforementioned 6-fold decrease of the dissociation constant. The estimated heat capacities (ΔC_P) of the complex formation for both peptides are quite similar, −0.21 and −0.22 kcal/K·mol for the unmodified and the Nek9 P-peptide, respectively. These values are in good agreement with the binding heat capacities estimated from the change in solvent-accessible surface area (SASA), −0.27 and −0.26 kcal/K·mol for the unmodified and

TABLE 3

Thermodynamic parameters for the binding of Nek9 peptides to LC8 (pH 7.5 and 25 °C)

Relative errors were 10% for K_a and K_d, 2% for ΔG, 5% for ΔH and $-T\Delta S$, and 10% for n_H.

	K_a	K_d[a]	ΔG[b]	ΔH[c]	$-T\Delta S$[d]	n_H[c]
	$\times 10^6\ M^{-1}$	μM	*kcal/mol*	*kcal/mol*	*kcal/mol*	
Nek9 peptide	6.2	0.16	−9.3	−11.2	1.9	0.16
Nek9 P-peptide	1.0	0.96	−8.2	−9.5	1.3	0.26

[a] $K_d = 1/K_a$.
[b] $\Delta G = -RT(\ln K_a)$.
[c] ΔH is the buffer-independent binding enthalpy, and n_H is the net number of exchanged protons between the complex and the bulk solvent upon ligand binding. These two parameters are estimated by linear regression from the observed binding enthalpies, ΔH_{obs}, in experiments performed using buffers with different ionization enthalpies, $\Delta H_{B(ion)}$, using this relationship: $\Delta H_{obs} = \Delta H + n_H \Delta H_{B(ion)}$.
[d] $-T\Delta S = \Delta G - \Delta H$.

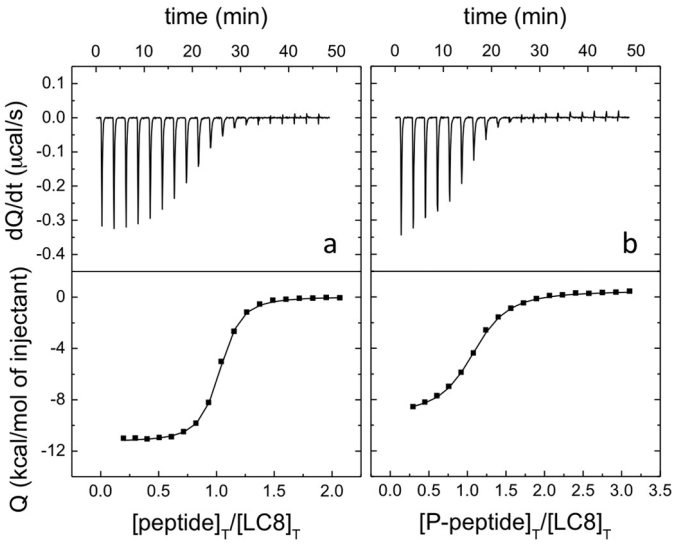

FIGURE 6. **Calorimetric titrations (isothermal titration calorimetry) for the LC8 binding to Nek9 peptides and Nek9 P-peptide.** Shown are calorimetric thermograms (*upper panels*, thermal power *versus* time) and binding isotherms (*lower panels*, normalized heat *versus* molar ratio) for the titration of LC8 10 μM with 200 μM Nek9 peptide (*a*) and 300 μM Nek9 P-peptide (*b*), in 100 mM NaCl, 10 mM sodium phosphate, 7.5 and 1 mM β-mercaptoethanol, at 25 °C.

the Nek9 P-peptide, respectively, employing a well known structural parameterization of the binding energetics in proteins ($\Delta C_P = 0.45 \times \Delta SASA_{nonpolar} - 0.26 \times \Delta SASA_{polar}$) (43) and the crystallographic structures of the complexes and apoLC8. These values indicate that there are not substantial conformational changes in LC8 upon binding of the peptides.

DISCUSSION

Post-translational modification of proteins by phosphorylation is one the most, if not the most, important manner of regulating protein-protein interactions and many signaling pathways inside of the cell (44). DYNLL/LC8 has been recently postulated to be a dimerization hub that can control the function of other proteins by regulating their oligomerization state, normally by inducing higher oligomerization states (13, 21). This might be the case for the protein kinase Nek9, which is involved in the control of early events of mitosis, and it has been shown to interact with LC8 through a canonical consensus region located in a partially disordered region of the C-terminal tail. In addition, LC8 negatively controls the binding of Nek9 to the related kinases Nek6/7 and thus their activation (12), suggesting that LC8 binding may have additional functions in the context of specific complexes besides regulating oligomerization. Thus, the regulation of LC8 binding might represent an important event to control the function of the target protein, in this case Nek9 and the formation of the mitotic spindle. In a recent work, we showed that Nek9 autophosphorylation on Ser^{944} may impair the interaction with LC8 *in vivo*, thus supporting the view that phosphorylation of LC8 binding partners can have a major effect in regulating the LC8 interaction (12). A similar LC8-mediated regulation was described for the proapoptotic Bim, which is sequestered to the LC8·dynein motor complexes but can be released upon phosphorylation by JNK kinase on the LC8 binding consensus motif. In this case, phosphorylation occurs on threonines adjacent to the central glutamine residue of the LC8 binding motif (45).

Examples describing the interaction of different partners to LC8 such as Dynein intermediate chain and Swallow (46, 47), indicate that LC8 seems to facilitate the folding and increase the α-helical content by stabilization of coiled-coil structures in those proteins. This "chaperone-like activity" of LC8 normally occurs in proteins with coiled-coil regions next to the LC8 binding consensus motif; those regions are normally intrinsically or partially disordered. In those examples, binding of LC8 can thus facilitate the formation of coiled-coil structures and thus dimerization of protein targets. In the case of dynein, in which LC8 was first described to act as a cargo adapter, this chaperone-like activity effect of LC8, which indirectly affects the cargo binding, has also been described (46, 48). In this case, the dynein intermediate chain is partially disordered and gains structure upon binding to LC8. In Nek9, our CD experiments show a high content of α-helical structure at the C-terminal region (Nek9-CC constructs, Fig. 1), probably indicating the presence of the predicted coiled-coil structure (1). In our LC8/Nek9-CC binding experiments with two point mutants for the LC8 consensus-binding motif, we observed different CD spectra when compared with the wild-type Nek9-CC construct. It might be that LC8 binding to Nek9 produces changes in the stability of the predicted Nek9 coiled-coil, thus affecting the Nek9 oligomerization state, as suggested in previous experiments (12).

We have analyzed the LC8-Nek9 interaction by using different biophysical methods. CD is an optimal approach to determinate directly the interaction of the peptide to LC8 by the measurement of changes in the β-signal, which is the type of secondary structure formed upon binding of the peptide (22). The ~18-fold reduction in the K_d extracted from the CD experiments with the Nek9 P-peptide is a direct indication of the perturbation of the interaction produced by the presence of the phosphate group. In the thermal denaturation unfolding of LC8 complexes, chased by intrinsic fluorescence, the major enthalpy of the complex between LC8 and the unmodified Nek9 peptide indicates a major energy released for the disruption of the complex in comparison with the Nek9 P-peptide. Finally, the thermodynamic values extracted from isothermal titration calorimetry experiments also show a 6-fold decrease of the dissociation constant (K_d) for the Nek9 P-peptide, due basically to less favorable enthalpic interactions, probably indicating a reduction in the number of bonds formed in the complex. All three methods point to a direct perturbation of the complex between LC8 and Nek9 upon phosphorylation on Ser^{944}.

The crystal structures of LC8 with both Nek9 peptides shed light to the binding differences observed in the biophysical experiments. The interaction of both Nek9 peptides to LC8 is carried out by a similar β-like antiparallel strand, which starts seven N-terminal positions to Gln^{948}, namely from Gly^{941} to Thr^{949}, forming a total number of eight backbone β-sheet hydrogen bonds between the Nek9 peptide and β3 strand of LC8 (see Fig. 2). However, comparisons between the six LC8 monomers in the asymmetric unit indicate that the phosphate negative charge on Ser^{944} perturbs the interaction with LC8, displaying a high degree of flexibility that affects mainly the

binding of the first half of the peptide, from positions −7 to −4 (Gly^{941} to Ser^{944}). The position of Ser^{944} in the LC8 binding motif of Nek9 is located four positions N-terminal to the central Gln^{948} and varies from Asp, Ser, Asn and Thr in the consensus sequence analysis for LC8 binding partners (13). Interestingly, some of them are either residues susceptible of being phosphorylated or residues with an inherent negative charge.

Despite the lower affinity for the Nek9 P-peptide and the important binding differences described *in vivo* (12), the high protein concentration in crystals favors the formation of fairly similar LC8·Nek9 complex structures. However, such high concentration of proteins are difficult to occur in the cellular context, and the reported K_d values strongly suggest that the differences between the unmodified and the Nek9 P-peptide are sufficient to perturb binding *in vivo*. The slight shift observed in the LC8 homodimer interface, the two disrupted hydrogen bonds in the Nek9 P-peptide complex and the higher flexibility of the Nek9 P-peptides produces a binding reduction on LC8 upon Ser^{944} phosphorylation.

We thus provide for the first time *in vitro* experimental data directly indicating that phosphorylation can regulate the binding of LC8 to a particular protein partner, in this instance, Nek9. Regulation of protein-protein interaction by phosphorylation is one of the most common ways to regulate many cellular signaling pathways. In the case of the mitotic Nek9/Nek6/Nek7 signaling module, LC8 seems to interfere in this pathway by a direct binding competition with the downstream kinases Nek6 and Nek7, regulation that can be reversed by direct phosphorylation on the interface between the two proteins. The fact that LC8 has multiple binding partners, that it is ubiquitously present, and that many of its protein partners contain Ser/Thr residues in the consensus binding motif, suggest that phosphorylation on this motif might be a general mechanism of controlling LC8 interaction in different cellular contexts.

Acknowledgments—We acknowledge Salvador Ventura for suggestions and stimulating discussions. We acknowledge Jordi Benach and Jordi Juanhuix from the XALOC beamline (BL13) at the ALBA synchrotron for help in data collection.

REFERENCES

1. Roig, J., Mikhailov, A., Belham, C., and Avruch, J. (2002) Nercc1, a mammalian NIMA-family kinase, binds the Ran GTPase and regulates mitotic progression. *Genes Dev.* **16,** 1640–1658
2. O'Connell, M. J., Krien, M. J., and Hunter, T. (2003) Never say never. The NIMA-related protein kinases in mitotic control. *Trends Cell Biol.* **13,** 221–228
3. Quarmby, L. M., and Mahjoub, M. R. (2005) Caught Nek-ing: cilia and centrioles. *J. Cell Sci.* **118,** 5161–5169
4. O'regan, L., Blot, J., and Fry, A. M. (2007) Mitotic regulation by NIMA-related kinases. *Cell Div.* **2,** 25
5. Roig, J., Groen, A., Caldwell, J., and Avruch, J. (2005) Active Nercc1 protein kinase concentrates at centrosomes early in mitosis and is necessary for proper spindle assembly. *Mol. Biol. Cell* **16,** 4827–4840
6. Bertran, M. T., Sdelci, S., Regué, L., Avruch, J., Caelles, C., and Roig, J. (2011) Nek9 is a Plk1-activated kinase that controls early centrosome separation through Nek6/7 and Eg5. *EMBO J.* **30,** 2634–2647
7. Rapley, J., Nicolàs, M., Groen, A., Regué, L., Bertran, M. T., Caelles, C., Avruch, J., and Roig, J. (2008) The NIMA-family kinase Nek6 phosphorylates the kinesin Eg5 at a novel site necessary for mitotic spindle formation. *J. Cell Sci.* **121,** 3912–3921
8. Belham, C., Roig, J., Caldwell, J. A., Aoyama, Y., Kemp, B. E., Comb, M., and Avruch, J. (2003) A mitotic cascade of NIMA family kinases. Nercc1/Nek9 activates the Nek6 and Nek7 kinases. *J. Biol. Chem.* **278,** 34897–34909
9. Sdelci, S., Bertran, M. T., and Roig J. (2011) Nek9, Nek6 and Nek7 and the separation of centrosomes. *Cell Cycle* **10,** 3816–3817
10. Yissachar, N., Salem, H., Tennenbaum, T., and Motro, B. (2006) Nek7 kinase is enriched at the centrosome, and is required for proper spindle assembly and mitotic progression. *FEBS Lett.* **580,** 6489–6495
11. Sdelci, S., Schütz, M., Pinyol, R., Bertran, M. T., Regué, L., Caelles, C., Vernos, I., and Roig, J. (2012) Nek9 phosphorylation of NEDD1/GCP-WD contributes to Plk1 control of gamma-tubulin recruitment to the mitotic centrosome. *Curr. Biol.* **22,** 1516–1523
12. Regué, L., Sdelci, S., Bertran, M. T., Caelles, C., Reverter, D., and Roig, J. (2011) DYNLL/LC8 protein controls signal transduction through the Nek9/Nek6 signaling module by regulating Nek6 binding to Nek9. *J. Biol. Chem.* **286,** 18118–18129
13. Rapali, P., Szenes, Á., Radnai, L., Bakos, A., Pál, G., and Nyitray, L. (2011) DYNLL/LC8: a light chain subunit of the dynein motor complex and beyond. *FEBS J.* **278,** 2980–2996
14. King, S. M., and Patel-King, R. S. (1995) The M(r) = 8,000 and 11,000 outer arm dynein light chains from *Chlamydomonas flagella* have cytoplasmic homologues. *J. Biol. Chem.* **270,** 11445–11452
15. King, S. M., Barbarese, E., Dillman, J. F., 3rd, Benashski, S. E., Do, K. T., Patel-King, R. S., and Pfister, K. K. (1998) Cytoplasmic dynein contains a family of differentially expressed light chains. *Biochemistry* **37,** 15033–15041
16. Benashski, S. E., Harrison, A., Patel-King, R. S., and King, S. M. (1997) Dimerization of the highly conserved light chain shared by dynein and myosin V. *J. Biol. Chem.* **272,** 20929–20935
17. Kaiser, F. J., Tavassoli, K., Van den Bemd, G. J., Chang, G. T., Horsthemke, B., Möröy, T., and Lüdecke, H. J. (2003) Nuclear interaction of the dynein light chain LC8a with the TRPS1 transcription factor suppresses the transcriptional repression activity of TRPS1. *Hum. Mol. Genet.* **12,** 1349–1358
18. Puthalakath, H., Huang, D. C., O'Reilly, L. A., King, S. M., and Strasser, A. (1999) The proapoptotic activity of the Bcl-2 family member Bim is regulated by interaction with the dynein motor complex. *Mol. Cell* **3,** 287–296
19. Jaffrey, S. R., and Snyder, S. H. (1996) PIN: an associated protein inhibitor of neuronal nitric oxide synthase. *Science* **274,** 774–777
20. Schnorrer, F., Bohmann, K., and Nüsslein-Volhard, C. (2000) The molecular motor dynein is involved in targeting swallow and bicoid RNA to the anterior pole of *Drosophila* oocytes. *Nat. Cell Biol.* **2,** 185–190
21. Barbar, E. (2008) Dynein light chain LC8 is a dimerization hub essential in diverse protein networks. *Biochemistry* **47,** 503–508
22. Liang, J., Jaffrey, S. R., Guo, W., Snyder, S. H., and Clardy, J. (1999) Structure of the PIN/LC8 dimer with a bound peptide. *Nat. Struct. Biol.* **6,** 735–740
23. Fan, J., Zhang, Q., Tochio, H., Li, M., and Zhang, M. (2001) Structural basis of diverse sequence-dependent target recognition by the 8 kDa dynein light chain. *J. Mol. Biol.* **306,** 97–108
24. Benison, G., Karplus, P. A., and Barbar, E. (2008) The interplay of ligand binding and quaternary structure in the diverse interactions of dynein light chain LC8. *J. Mol. Biol.* **384,** 954–966
25. Lightcap, C. M., Sun, S., Lear, J. D., Rodeck, U., Polenova, T., and Williams, J. C. (2008) Biochemical and structural characterization of the Pak1-LC8 interaction. *J. Biol. Chem.* **283,** 27314–27324
26. Wang, W., Lo, K. W., Kan, H. M., Fan, J. S., and Zhang, M. (2003) Structure of the monomeric 8-kDa dynein light chain and mechanism of the domain-swapped dimer assembly. *J. Biol. Chem.* **278,** 41491–41499
27. Makokha, M., Huang, Y. J., Montelione, G., Edison, A. S., and Barbar, E. (2004) The solution structure of the pH-induced monomer of dynein light-chain LC8 from *Drosophila*. *Protein Sci.* **13,** 727–734
28. Mohan, P. M., Barve, M., Chatterjee, A., and Hosur, R. V. (2006) pH driven conformational dynamics and dimer-to-monomer transition in DLC8. *Protein Sci.* **15,** 335–342
29. Song, Y., Benison, G., Nyarko, A., Hays, T. S., and Barbar, E. (2007) Potential role for phosphorylation in differential regulation of the assembly of

dynein light chains. *J. Biol. Chem.* **282,** 17272–17279
30. Jung, Y., Kim, H., Min, S. H., Rhee, S. G., and Jeong, W. (2008) Dynein light chain LC8 negatively regulates NF-κB through the redox-dependent interaction with IκBα. *J. Biol. Chem.* **283,** 23863–23871
31. Song, C., Wen, W., Rayala, S. K., Chen, M., Ma, J., Zhang, M., and Kumar, R. (2008) Serine 88 phosphorylation of the 8-kDa dynein light chain 1 is a molecular switch for its dimerization status and functions. *J. Biol. Chem.* **283,** 4004–4013
32. Lo, K. W., Naisbitt, S., Fan, J. S., Sheng, M., and Zhang, M. (2001) The 8-kDa dynein light chain binds to its targets via a conserved (K/R)*X*TQT motif. *J. Biol. Chem.* **276,** 14059–14066
33. Rodríguez-Crespo, I., Yélamos, B., Roncal, F., Albar, J. P., Ortiz de Montellano, P. R., and Gavilanes, F. (2001) Identification of novel cellular proteins that bind to the LC8 dynein light chain using a pepscan technique. *FEBS Lett.* **503,** 135–141
34. Radnai, L., Rapali, P., Hódi, Z., Süveges, D., Molnár, T., Kiss, B., Bécsi, B., Erdödi, F., Buday, L., Kardos, J., Kovács, M., and Nyitray, L. (2010) Affinity, avidity, and kinetics of target sequence binding to LC8 dynein light chain isoforms. *J. Biol. Chem.* **285,** 38649–38657
35. Gómez, J., and Freire, E. (1995) Thermodynamic mapping of the inhibitor site of the aspartic protease endothiapepsin. *J. Mol. Biol.* **252,** 337–350
36. Velazquez-Campoy, A., Luque, I., Todd, M. J., Milutinovich, M., Kiso, Y., and Freire, E. (2000) Thermodynamic dissection of the binding energetics of KNI-272, a potent HIV-1 protease inhibitor. *Protein Sci.* **9,** 1801–1809
37. Kabsch, W. (2010) XDS. *Acta Crystallogr. D Biol. Crystallogr.* **66,** 125–132
38. Winn, M. D., Ballard, C. C., Cowtan, K. D., Dodson, E. J., Emsley, P., Evans, P. R., Keegan, R. M., Krissinel, E. B., Leslie, A. G., McCoy, A., McNicholas, S. J., Murshudov, G. N., Pannu, N. S., Potterton, E. A., Powell, H. R., Read, R. J., Vagin, A., and Wilson, K. S. (2011) Overview of the CCP4 suite and current developments. *Acta Crystallogr. D Biol. Crystallogr.* **67,** 235–242
39. Emsley, P., Lohkamp, B., Scott, W. G., and Cowtan, K. (2010) Features and development of Coot. *Acta Crystallogr. D Biol. Crystallogr.* **66,** 486–501
40. Adams, P. D., Afonine, P. V., Bunkóczi, G., Chen, V. B., Davis, I. W., Echols, N., Headd, J. J., Hung, L. W., Kapral, G. J., Grosse-Kunstleve, R. W., McCoy, A. J., Moriarty, N. W., Oeffner, R., Read, R. J., Richardson, D. C., Richardson, J. S., Terwilliger, T. C., and Zwart, P. H. (2010) PHENIX: a comprehensive Python-based system for macromolecular structure solution. *Acta Crystallogr. D Biol. Crystallogr.* **66,** 213–221
41. DeLano, W. L. (2010) *The PyMOL Molecular Graphics System*, version 1.3, Schrödinger, LLC, New York
42. Benison, G., Karplus, P. A., and Barbar, E. (2007) Structure and dynamics of LC8 complexes with KXTQT-motif peptides: swallow and dynein intermediate chain compete for a common site. *J. Mol. Biol.* **371,** 457–468
43. Murphy, K. P., and Freire, E. (1992) Thermodynamics of structural stability and cooperative folding behavior in proteins. *Adv. Protein Chem.* **43,** 313–361
44. Manning, G., Whyte, D. B., Martinez, R., Hunter, T., and Sudarsanam, S. (2002) The protein kinase complement of the human genome. *Science* **298,** 1912–1934
45. Lei, K., and Davis, R. J. (2003) JNK phosphorylation of Bim-related members of the Bcl2 family induces Bax-dependent apoptosis. *Proc. Natl. Acad. Sci. U.S.A.* **100,** 2432–2437
46. Wang, L., Hare, M., Hays, T. S., and Barbar, E. (2004) Dynein light chain LC8 promotes assembly of the coiled-coil domain of swallow protein. *Biochemistry* **43,** 4611–4620
47. Nyarko, A., Hare, M., Hays, T. S., and Barbar, E. (2004) The intermediate chain of cytoplasmic dynein is partially disordered and gains structure upon binding to light-chain LC8. *Biochemistry* **43,** 15595–15603
48. Benison, G., Nyarko, A., and Barbar, E. (2006) Heteronuclear NMR identifies a nascent helix in intrinsically disordered dynein intermediate chain: implications for folding and dimerization. *J. Mol. Biol.* **362,** 1082–1093